Progress In Electromagnetics Research M, Vol. 55, 73–84, 2017

Evaluation of Hybrid Polarimetric Decomposition Techniques for Winter Crop Discrimination

Sanid Chirakkal*, Dipanwita Haldar, and Arundhati Misra

Abstract—In this paper we compare, using ISRO's RISAT-1 FRS-1 mode Compact Polarimetric (CL-Pol) data, two widely used hybrid polarimetric decomposition techniques, $m-\delta$ and $m-\chi$ decompositions, with regard to classification accuracy for various agricultural crops of north and west India. We show that the classification based on the $m-\chi$ decomposition results in better crop separability in general. But the crop stage and existence of orientating structures in the crops affects the efficacy of decomposition; a fact vividly brought out in this paper. Theoretical insights into the effectiveness of these decomposition techniques for different crop geometry are brought forth. We also compare the classification accuracy subsequent to polarimetric speckle filtering vis-a-vis spatial multilooking (downsampling). We show that usage of an appropriate polarimetric filter tends to produce comparable accuracy for most of the agricultural classes, as that of multilook case, without degrading spatial resolution. This work showcases a custom implementation of Stokes parameter based decomposition as well as POLSAR filter based on refined Lee algorithm, written in C and tailored to RISAT-1.

1. INTRODUCTION

RISAT-1 (Radar Imaging Satellite) SAR of Indian Space Research Organization (ISRO) operates in Compact Polarimetric (CL-Pol) mode, which provides some fundamental advantages over fully polarimetric SAR. Such a radar has lower hardware cost and is relatively easy to implement. Moreover, CL-Pol SAR has lower susceptibility to noise and cross-channel errors [1, 2]. A radar in CL-Pol architecture transmits circularly polarized electromagnetic waves and receives two orthogonal linear polarizations. One advantage of this is that the received total power in the orthogonal basis will be rotationally invariant with respect to orientation of elementary scatterers in the scene. This is so because the transmitted wave is circularly polarized and hence does not favor any particular orientation. RISAT-1 SAR with CL-Pol is the first such SAR for earth observation mission, before which such an architecture was used in Mini-SAR of Chandrayaan-1 and the Mini-RF on the Lunar Reconnaissance Orbiter for lunar studies. Advantage of CL-Pol for various applications has been demonstrated in [3, 4] with reference to oceanic and terrestrial features.

Various studies in literature focus on the worthiness of CL-Pol architecture for polarimetric decomposition and feature classifications [3, 5, 6]. The similarity in the scattering representations between fully polarimetric and compact polarimetric data makes it possible to apply polarimetric decomposition techniques to data acquired from one mode to data acquired from the other mode [3]. $\pi/4$ mode simulated by Lardeux et al. [15] resulted in the overall classification performance similar (κ lower of 3%) to those observed with full polarimetric data, with a higher confusion for the Pinus class. The hybrid

Received 16 January 2016, Accepted 14 February 2017, Scheduled 14 March 2017

* Corresponding author: Sanid Chirakkal (sanid@sac.isro.gov.in).

The authors are with the Microwave and Hyperspectral Techniques Development Division, Geo-Sciences, Hydrology, Cryosphere Sciences and Applications Group, Space Applications Centre, Indian Space Research Organization, Ahmedabad, Gujarat 380 015, India.

polarimetric modes data such as 'the $\pi/4$ mode' and 'circular transmit linear orthogonal receive modes (CTLR)' synthesized from full-polarimetric data showed intermediate classification accuracy (79%–81.5%) [17]. Moreover, the $\pi/4$ mode shows much better performance for the land use discrimination of the studied scene than ENVISAT Alternate Polarisation modes involving intensities acquired in co- or cross-polarization [14]. When only single-date data set is available, the CL-Pol with its different toolkit of decomposition techniques has promising potential for crop classification compared to single- or dual-polarized SAR data.

The information contained in the CL-Pol backscatter can be fully captured in the four Stokes parameters (g_0, g_1, g_2, g_3). From these, other parameters of interest can be calculated, such as the degree of polarization (m), coherency parameter $(|\mu_{xy}|)$, circular polarization ratio (μ_c) and relative phase (δ) between two electric vectors in the backscattered field. Here, we give a brief outline of these quantities and then proceed to show the $m-\delta$ and $m-\chi$ decomposition strategies for RISAT-1 data.

2. THE POLARIMETRIC FILTER AND POLARIMETRIC DECOMPOSITION METHODS

Speckle filtering algorithm for a single polarization SAR data has matured over the past two decades. Earlier approaches, based on Fourier analysis, tend to degrade the image due to low-pass filtering in the frequency domain. Later algorithms tried to achieve speckle reduction without sacrificing the image quality. Such filters were generally implemented in spatial domain, not in frequency domain. In 1980, Lee [7] developed a filter based on local statistics, which was later refined [8] by adopting edge aligned windows. Polarimetric speckle filters are specifically designed to preserve the statistical properties of covariance matrix, as in the case of spatial multilooking. They also avoid cross-talk between polarization channels, brought about by the process of speckle filtering. One such approach was put forth by Lee et al. [9], which filters the covariance matrix by using edge-aligned nonsquare windows and applying a minimum mean square error (MMSE) filter. The filtering weights as well as the edge aligned windows are selected using the span image.

We assume a multiplicative noise model for SAR speckle noise, where the amplitude of an SAR image at (i,j)th pixel, $y(i,j)$, is written as:

$$y(i,j) = x(i,j)\mu(i,j), \tag{1}$$

where $x(i,j)$ is the noise-free backscatter amplitude and $\mu(i,j)$ the Gaussian noise with mean 1 and standard deviation σ_μ. Now MMSE reduces the mean square error between the estimated x $(\tilde{x})$ and actual x by minimizing the mean square error using the function,

$$\tilde{x} = a\bar{x} + by, \tag{2}$$

where $\bar{x}$ is evaluated by the local mean of y in a predefined window. This fixes the coefficients in Equation (2) in terms of mean and variance of the SAR amplitude image (y) computed in a local window and the standard deviation of the Gaussian noise, μ.

$$\tilde{x} = \bar{y} + b(y - \bar{y}), \tag{3}$$

where b, given by

$$b = \frac{Var(x)}{Var(y)}, \tag{4}$$

is the weight between local mean and original pixel value. In Equation (4), variance of x is given by:

$$Var(x) = \frac{Var(y) - \bar{y}^2\sigma_\mu^2}{(1+\sigma_\mu^2)}. \tag{5}$$

MMSE is an adaptive filter and is further refined by using edge-aligned non-square windows instead of using fixed window geometry in the case of refined Lee filter. In the case of polarimetric refined Lee filter, instead of filtering the amplitude image the covariance matrix (C_2 in the case of CL-pol data) is filtered using the span image (sum of diagonal elements). The filter weight defined earlier in

Equation (4) is computed from the span image, and the same is applied to all the elements of covariance matrix independently. This gives rise to a vector form of Equation (3) [10],

$$\tilde{\mathbf{X}} = \bar{\mathbf{Y}} + b\left(\mathbf{Y} - \bar{\mathbf{Y}}\right), \tag{6}$$

where each element of $\bar{\mathbf{Y}}$ is the local mean of elements of C_2, calculated from the same exact edge aligned windows. In this paper, we use the POLSAR refined Lee filter with a moving 9×9 edge-aligned window for filtering. Another (simpler) approach to deal with speckle noise, which is very commonly employed in SAR processing, is spatial multilooking (downsampling). This is done by averaging the neighboring pixels in an amplitude image by a boxcar filter. This reduces the speckle noise considerable at the cost of degrading the spatial resolution.

RISAT-1 FRS-1 (Fine Resolution Mode) uses right circularly polarized wave transmission, and the backscattered signal is received in coherent dual polarizations (these channels are called RH and RV). The relative phase difference between the RH and RV channels is preserved making it a polarimetric mode. In the case of electromagnetic wave propagation through a linear medium devoid of moving electric charges, it is shown that a general solution to Maxwell's equation is that of a monochromatic elliptically polarized wave [11]. That is, if we take any plane normal to the propagation vector $\mathbf{k}$, we see that, as time advances, the tip of electric vector traces out an ellipse in this plane. This ellipse (called polarization ellipse) can be characterized using three parameters, the ellipse amplitude (A), ellipse orientation angle (ϕ) and ellipticity angle (χ). These parameters are pictorially represented in Figure 1.

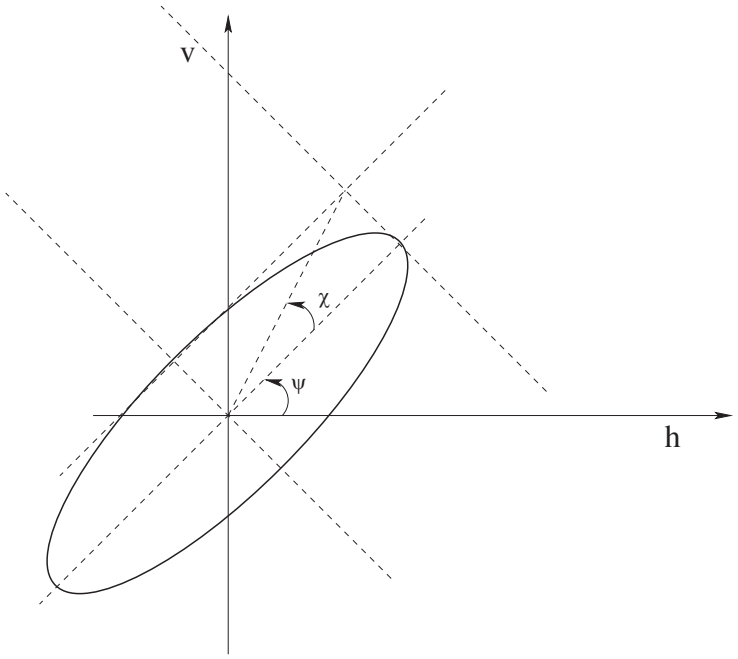

Figure 1. Pictorial representation of the polarization ellipse and the angles ψ and χ.

Another way to characterize polarization of a wave, especially in the case of partially polarized wave, is through Stokes parameters. The Stokes parameters for a CL-Pol architecture is given by [1]:

$$\begin{aligned} g_0 &= \left\langle |E_{RH}|^2 + |E_{RV}|^2 \right\rangle \\ g_1 &= \left\langle |E_{RH}|^2 - |E_{RV}|^2 \right\rangle \\ g_2 &= 2\mathrm{Re}\left\langle E_{RH} E_{RV}^* \right\rangle \\ g_3 &= -2\mathrm{Im}\left\langle E_{RH} E_{RV}^* \right\rangle, \end{aligned} \tag{7}$$

where E is the complex voltage, and Re stands for real part and Im for imaginary one of the complex

number. For a fully polarized wave, we have the following equality:

$$g_0^2 = g_1^2 + g_2^2 + g_3^2. \tag{8}$$

The Stokes parameters can be related to polarization ellipse parameters through the following equations:

$$\begin{aligned} g_1 &= g_0 \cos(2\chi)\cos(2\psi) \\ g_2 &= g_0 \cos(2\chi)\sin(2\psi) \\ g_3 &= g_0 \sin(2\chi). \end{aligned} \tag{9}$$

From the Stokes parameters, various auxiliary parameters can be computed. The degree of polarization (m) is given by:

$$m = \frac{\sqrt{g_1^2 + g_2^2 + g_3^2}}{g_0}. \tag{10}$$

Similarly, relative phase, δ, is given by:

$$\delta = \arctan\left(\frac{g_3}{g_2}\right). \tag{11}$$

For a fully polarized EM field ($m = 1$) and Stokes parameters, locate a point on the surface of a unit sphere, called Poincare sphere [12]. If the backscatter field is partially polarized (which is usually the case), the degree of polarization will be less than unity, and Stokes parameters determine a specific point on the surface of a sphere with coordinates (mg_0, χ, ψ). The parameter χ is calculated as follows:

$$\sin(2\chi) = \frac{-g_3}{mg_0} \tag{12}$$

The $m-\delta$ decomposition is achieved using three inputs, viz., the first Stokes parameter g_0 (representing total back-scattered power), relative phase δ, and degree of polarization m. The decomposition defined in Equation (13) can be presented under a RGB color composite representation where V_R, V_G and V_B correspond to even bounce scattering, volume scattering and odd bounce scattering, respectively [12, 13].

$$\begin{pmatrix} V_R \\ V_G \\ V_B \end{pmatrix} = \begin{pmatrix} \sqrt{g_0 m \dfrac{(1-\sin\delta)}{2}} \\ \sqrt{g_0(1-m)} \\ \sqrt{g_0 m \dfrac{(1+\sin\delta)}{2}} \end{pmatrix} \tag{13}$$

Another polarimetric decomposition closely related to the $m-\delta$ decomposition is $m-\chi$ decomposition. The $m-\chi$ decomposition is achieved making use of the ellipticity angle χ as opposed to the relative phase δ. This decomposition is defined by Equation (14).

$$\begin{pmatrix} V_R \\ V_G \\ V_B \end{pmatrix} = \begin{pmatrix} \sqrt{g_0 m \dfrac{(1+\sin 2\chi)}{2}} \\ \sqrt{g_0(1-m)} \\ \sqrt{g_0 m \dfrac{(1-\sin 2\chi)}{2}} \end{pmatrix} \tag{14}$$

In this study, we use RISAT-1 FRS1 mode data over Haryana region acquired in March 2013 to study the odd bounce, even bounce and volumetric scattering decomposition based on $m-\delta$ and $m-\chi$. The algorithm makes use of Stokes parameters and auxiliary quantities directly derived out of it. We use polarimetric refined Lee filter with 9×9 moving window for denoising the image. The decomposition is performed on a slant range L1 data product of RISAT-1. To compare the output of polarimteric filter with the spatial-multilook processing, we produce output by 6×4 multilooking (this is found to be the optimal factor by experience). The end-to-end processing is done using a in-house developed polarimetric processing tool. A flowchart depicting the process flow is given in Figure 2. The RGB composite is exported using GDAL (Geospatial Data Abstraction Library), and subsequently ENVI® software is used for maximum likelihood classification. The specification of the RISAT-1 data products is given in Table 1. The details can be seen in [16].

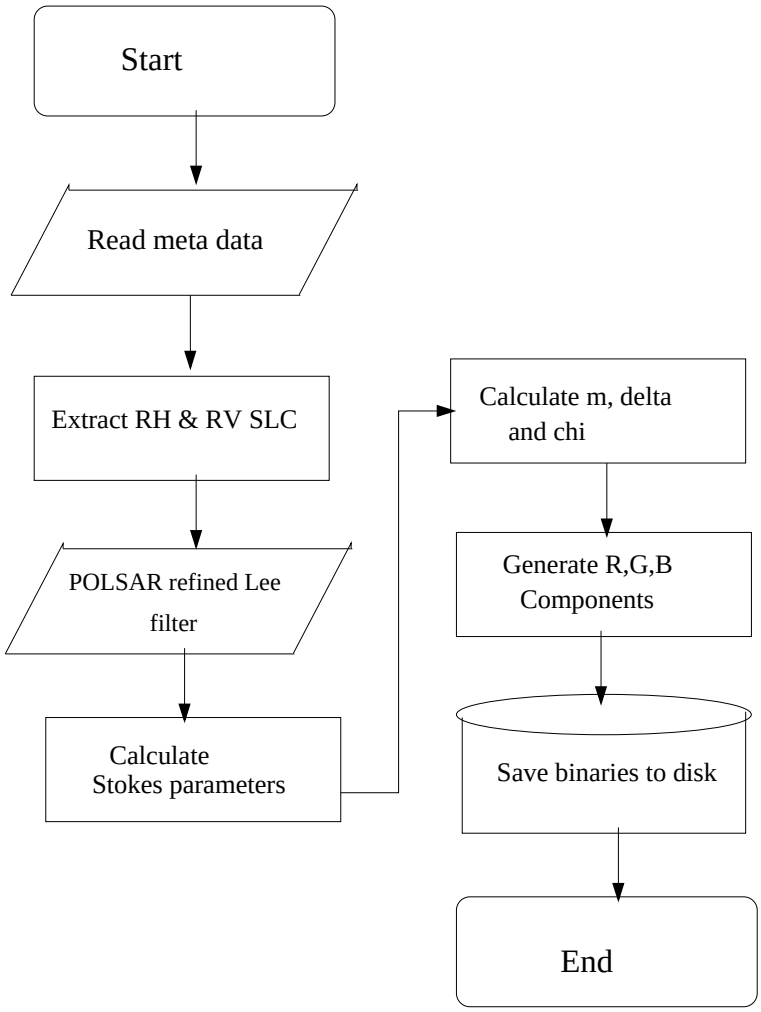

Figure 2. Process flow for generating polarimetric decomposed images starting from RISAT-1 FRS-1 CP image in CEOS format.

Table 1. Specifications of RISAT-1 data used for the study.

Serial #	Property	Value
1	Orbit	Circular polar sun synchronous
2	Orbit altitude	536 km
3	Orbit inclination	97.552°
4	Date of pass	27-MAR-2013
5	Image format	CEOS
6	Processing level	SLC
7	Incidence angle (deg)	43.395
8	TxRxPol1	RV
9	TxRxPol2	RH

3. STUDY AREA AND GROUND TRUTH

Central State Farm located in Hisar district of Haryana (India) has been selected for the present study. The area is bounded by the coordinates $29^\circ\ 11' - 29^\circ\ 20'\ N$ latitudes and $75^\circ\ 36' - 75^\circ\ 45'\ E$ longitudes.

This is a farmland of considerable size where large experimental crop fields (more than 5 ha) are maintained for seed generation and distribution to the state farmers. The major agricultural crops grown in this area include rice, cotton and pulses during Indian *kharif* (summer/monsoon) season and wheat, mustard, gram (chick pea), peas during Indian *rabi* (winter) season. In the present study, we analyse a *rabi* season dataset of RISAT FRS-1. The *rabi* season starts at the end of September when mustard sowing starts and continues till mid-October. The early wheat crop is sown in November and the late wheat sown during late December to January, after the harvest of cotton crop of previous *kharif* season in and adjacent to central state farm. The gram is sown during late October to early November. The high volume scattering component in the March image will correspond to the late wheat area dominantly, and other *rabi* crops in mature and advanced stage of growth will also have significantly surface component.

Ground truth data were collected by field survey during the acquisition periods synchronized with the satellite passes over the area, including collection of all important information of the crop type, stage, height, percentage cover, vigour, soil roughness and moisture status. GPS (Magellan NAVDLX-10) coordinates were noted during ground truth data collection for the above parameters. Sites having an area greater than 3 ha in contiguity of crop were selected for this purpose. In addition, ground truth information also contains other information related to the existing land cover features such as urban, other crops and vegetation, water bodies, plantation and forest. The information was collected at all the locations of 30 sites for mustard and wheat and 15 for gram.

4. FEATURE CLASSIFICATION USING $M-\delta$ AND $M-\chi$ DECOMPOSITION TECHNIQUES

The study area encompasses major winter crops such as wheat, mustard and gram. The other features are plantations, urban setups, water body, etc. Based on the decomposition outputs (RGB), which resulted in the segregation of various scattering components, supervised maximum likelihood classification was carried out to address the crop discrimination problem. The decomposed images represented in Figures 3(a), 3(b), 4(a) and 4(b) are the RGB composites where red stands for even bounce scattering, green for diffuse (depolarization) scattering and blue for odd bounce scattering.

For March 27 data, the date of acquisition coincides with a stage in which most of the crops are in advanced stage or on the verge of harvest. As shown in Table 2, $m-\chi$ decomposition based classification gives higher accuracy for most of the landcovers in general compared to the $m-\delta$ decomposition. This can be attributed to the fact that χ captures the ellipticity of the polarization ellipse, and for the advanced crop phase, we have isotropic scatters. For most of the classes, results are comparable for both these decomposition methods. Late sown wheat is sown by the end of December or early January in north India after the harvest of cotton crop. The $m-\delta$ uses the relative phase information of RH and

Table 2. Classification accuracy of various land covers in Central State Farm, Hisar, Haryana. (a) POLSAR filter. (b) Multi-look.

(a)

Features	$m-\delta$	$m-\chi$
Late wheat	77	86
Early wheat	59	78
Gram	83	82
Mustard	93	98
Mustard late	97	97
Water body	100	100
Urban	98	99
Plantations	97	98
Bare soil	100	100

(b)

Features	$m-\delta$	$m-\chi$
Late wheat	74	91
Early wheat	87	87
Gram	93	94
Mustard	93	94
Mustard late	83	88
Water body	100	100
Urban	100	100
Plantations	80	82
Bare soil	100	100

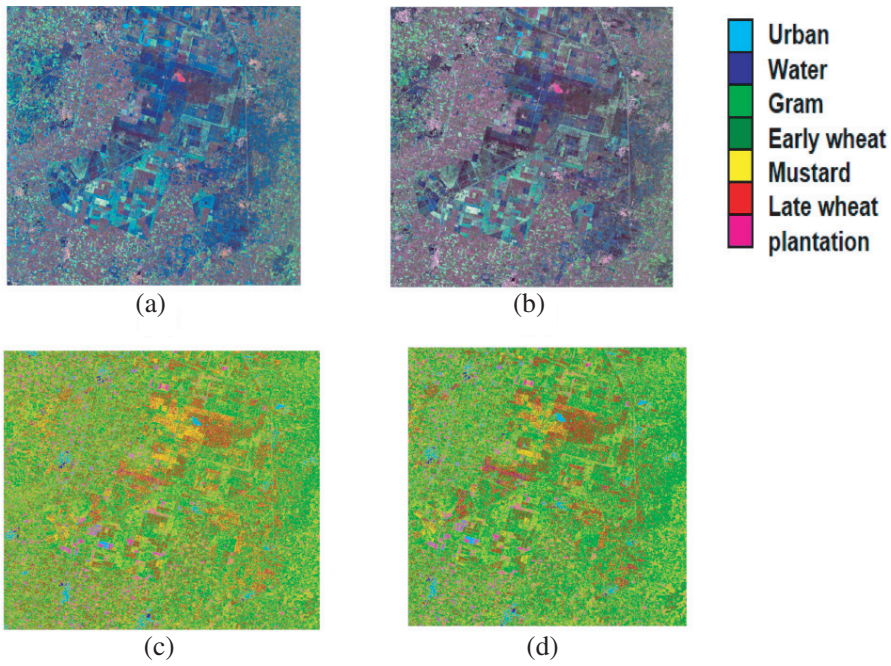

Figure 3. Stokes parameter based decomposition and classification output for 27 March, 2013, RISAT-1 compact polarimetric data, after applying polarimetric filter. (a) $m-\delta$ decomposed image. (b) $m-\chi$ decomposed image. (c) Classified image corresponding to $m-\delta$ decomposition. (d) Classified image corresponding to $m-\chi$ decomposition.

RV, precisely the H and V phase angles. For younger crops, the vertical component is less dominant, and the canopy appears to be an isotropic scatterer, in the first phase, till 50–60 days after sowing. Once the panicles emerge, the wheat fields resemble a uniform carpet of dense scatterers (the canopy) with periodic panicle stalks standing vertically over this carpet. Panicles are complex inflorescence, which is much branched. They act as scatterers inducing double or multiple bounces to microwave radar signal. The late sown wheat will have a directional component during late March due to panicle development whereas the early sown crop will be near maturity phase with matured panicles amidst the dry leaves. This directional effect for the late sown wheat results in better classification accuracy than the early/timely sown wheat in the $m-\delta$ decomposition [18]. The accuracy has been verified by the test data sites. This directionality distinction leads to separation of wheat in calendar year (November — sown early and January — sown late) due to their sowing date differences and plays an important role in terms of information for better separability among classes in both the $m-\chi$ and $m-\delta$ based decompositions. Late sown wheat is observed to be separated out from the early sown wheat with higher efficacy in both the $m-\chi$ and $m-\delta$ decomposition based classifications but more so in the $m-\delta$ decomposition (Table 2). We attribute this to the existence of orientating structures, panicles, in late wheat which induce double/multiple bounce scattering. This immediately affects the relative phase angle (δ) directly and hence the $m-\delta$ decomposition.

As can be inferred from Table 3 (omission/commision table [19]), late wheat is classified with higher accuracy than the early wheat, which has at least one month difference in the sowing dates. For most of the features, overall accuracies are higher in the $m-\chi$ case, leading to, in general, a better performer. In the spatial multilooking based classification as shown in Table 4, late wheat is again classified with lesser errors in general and commission in particular. This leads to higher accuracy for the late wheat. The late mustard crop fields, located outside the central farm, are a bunch of small, heterogeneous and scattered fields. Since this class is erroneously getting committed to the early wheat and early mustard class (here late mustard sowing calendar overlaps with early wheat sowing), the classification accuracy degrades while multilooking. This can be readily seen from the commission/omission matrix. This class is better separated in the POLSAR filtered full resolution dataset.

Table 3. $m-\delta$ and $m-\chi$ omission/commission error table for various features under the study.

	POLSAR filter			
	$m-\delta$		$m-\chi$	
Class	Commission	Omission	Commission	Omission
Urban	0	1.74	0	0.87
Water	0	0	0	0
Early mustard	31.63	6.29	2.76	1.4
Gram	10.7	18.44	9.8	17.34
Late wheat	11.95	23.08	13.66	13.19
Early wheat	23.3	40.6	20	21.8
Plantations	3.14	3.14	1.89	1.89
Late mustard	4.17	2.54	2.52	1.69
Bare Soil	0	0	0	0
	Multi-look			
	$m-\delta$		$m-\chi$	
Class	Commission	Omission	Commission	Omission
Urban	1.01	0.50	0	0
Water	0	0	0	0
Early mustard	28.06	6.54	5.61	5.61
Gram	9.8	17.34	6.8	7.34
Late	4.61	26.02	2.72	8.67
Early wheat	32.50	12.90	35.71	12.90
Plantations	7.14	20.41	4.76	18.37
Late mustard	40.35	17.07	35.71	12.20
Bare Soil	0	0	0	0

Degree of circularity forms the basis for decomposition in $m-\chi$ decomposition in addition to the degree of polarization and responds to the target well when the target is isotropic rather than directional, which applies to the early stage of the wheat crop as well as the very advanced stage of the crop. In the present investigation, early sown (sown during November early/mid) wheat crop is in advanced growth stage in March. This results in similar classification accuracy in both $m-\delta$ and $m-\chi$ decomposition based classifications due to their isotropic scattering mechanism especially observed in the multilook processing scenario (Table 2(b)). Overall higher classification accuracy is observed in $m-\chi$ case for both polarimetric filtered image and that by multilooking approach.

Mustard is sown earlier in season during late September to early October and harvested during late March/early April. During late March, most of the leaves are shed, and the plants are full of the siliqua, reaching maturity fast. The initial directional vertical component present in the mustard fields during 40–60 days after sowing is lost in the advanced stage of siliqua maturity. This effect of isotropic nature is added by the heavy branching habit and siliqua weight of the mustard crop. The isotropic scattering resulting in high classification accuracy in both $m-\delta$ and $m-\chi$ decomposition components. The accuracy in the $m-\chi$ case is slightly higher than the $m-\delta$, which is attributed to heavy and dense mustard canopy loaded with mature siliqua fruits. The late sown mustard is sown during first fortnight of October and follow a similar response to the timely sown mustard crop due to faster rate of growth initially. This is in contrary to the late sown wheat crop where there is distinct lag between the early and late sown remains due to the initially slower rate of growth. The $m-\chi$ gives a higher classification overall accuracy of 92% than 87% for the $m-\delta$.

Both $m-\chi$ and $m-\delta$ decomposition based classifications are useful at various crop stages depending on the stage, cultural practice and canopy geometry. Subtle differences in directional scattering is

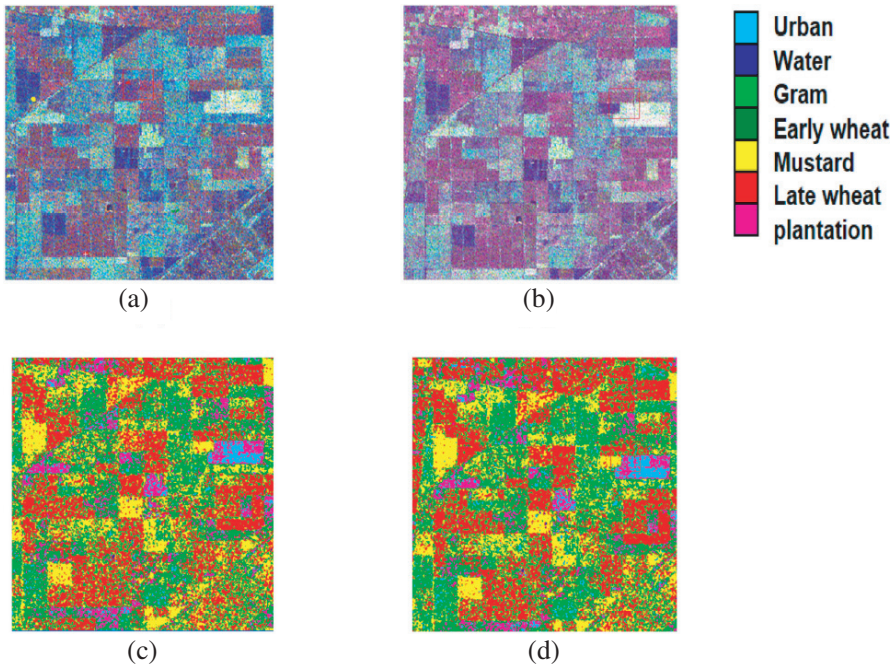

Figure 4. Stokes parameter based decomposition and classification output for 27 March, 2013, RISAT-1 compact polarimetric data. (a) $m-\delta$ decomposed image. (b) $m-\chi$ decomposed image. (c) Classified image corresponding to $m-\delta$ decomposition. (d) Classified image corresponding to $m-\chi$ decomposition.

reflected by $m-\delta$ whereas mature stage isotropic scatterers are brought out well by $m-\chi$ decomposition. Establishing this theoretically needs more hybrid polarimetric data evaluation that addresses various crops differing in stage and geometry. The preferential orientation of crop structures (vegetation), which can induce double or multiple scatterings to microwave radar signal, can be found coinciding with particular phenophase unique to each crop type. In such cases, $m-\delta$ decomposition is expected to perform well. In advanced crop stages and in multi-stage scenario as a whole $m-\chi$, decomposition performs well.

The polarimetric filter based classification retains the original spatial resolution of the data unlike the spatial multilooked processing. For the classification results of most of the landcovers, the polarimetric filtered processing is consistent with the multilook approach [20]. This is apparent from the present study as seen in Table 2. The early sown wheat is mostly grown in farmers' fields surrounding the central state farm and is heterogeneous in nature. Since multilooking reduces heterogeneity, the accuracies of both δ and χ based decompositions are correspondingly increased for this class. In homogeneous cases, like plantations and mustard, the decomposition subsequent to polarimetric filtering performs well.

The results presented so far are further corroborated with the results from a similar study using data over the major wheat growing region in the Junagad district of Gujrat (date of pass February 12, 2015). We again use FRS-1 hybrid polarimetric mode to showcase the reproducibility of our results over a different date of acquisition over an area with similar crops (Figure 5). Here again the late wheat is separated with higher accuracy in both $m-\delta$ and $m-\chi$ decompositions, as can be seen from Table 4. The other important crops are coriander, found mostly in the southern part of the scene, and cotton, which is in dried and harvesting phase, whereas cotton and coriander in advanced stages show similar accuracies for both $m-\chi$ and $m-\delta$, so do the early and late sown wheat, and the mid-season wheat shows better accuracy in $m-\delta$ decomposition. Orchards are found to be discriminated well by the $m-\delta$ method. This again leads to the conclusion already arrived from the Haryana state farm data set, viz., for an agricultural scenario, $m-chi$ decomposition gives an overall better accuracy, but there exist cases where $m-\delta$ shows more sensitivity to certain crop stages. For the downsampling versus POLSAR filter scenario we can also reproduce similar results using the Junagad data set (Table 4).

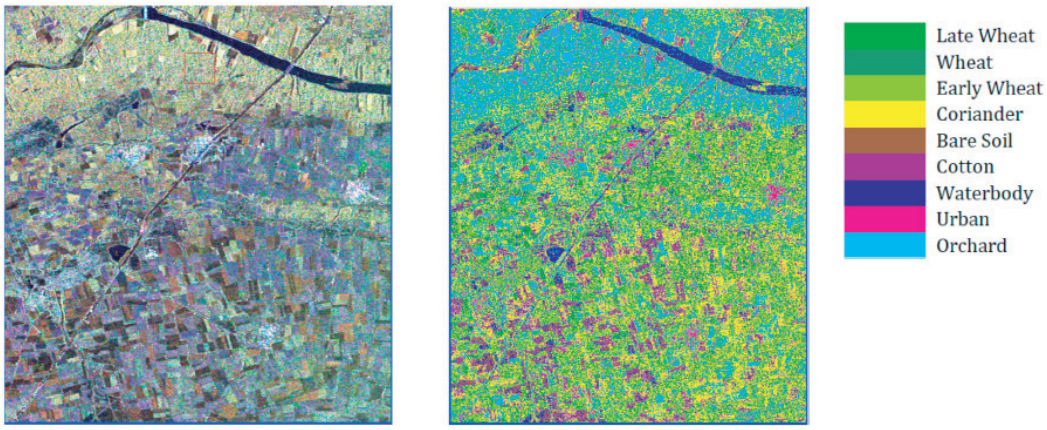

(a) (b)

Figure 5. Stokes parameter based decomposition and classification output for 12 February, 2015, CL-pol data over Junagad, Gujarat. (a) Full resolution POLSAR filtered and $m-\chi$ decomposed image. (b) Classified image corresponding to $m-\chi$ decomposition.

Table 4. Classification accuracy of various land covers in Junagad field, Gujarat. (a) POLSAR filter. (b) Multi-look.

(a)

Features	$m-\delta$	$m-\chi$
Late wheat	92	91
Early wheat	63	59
Wheat	53	63
Coriander	74	68
Cotton	85	85
Water body	84	91
Urban	100	100
Orchards	71	52
Bare soil	85	81

(b)

Features	$m-\delta$	$m-\chi$
Late wheat	95	91
Early wheat	48	59
Wheat	68	84
Coriander	97	97
Cotton	85	90
Water body	97	97
Urban	96	96
Orchards	84	81
Bare soil	94	98

5. CONCLUSION

The polarimetric decomposition of CL-Pol SAR data of ISRO's RISAT-1 FRS-1 mode (over Haryana state farm) was achieved using quantities derived out of Stokes parameters. A polarimetric speckle filter, based on refined Lee POLSAR filter, was implemented to denoise CL-Pol data. Two widely used hybrid polarimetric decomposition techniques, the $m-\delta$ and $m-\chi$ decompositions, were compared rigorously using an agricultural scene with ground validated data points. We show the significant result that usage of a polarimetric filter produces comparable classification accuracy to that of spatial multilook case, without degrading spatial resolution. The overall advantage of using $m-\chi$ over $m-\delta$ for advanced stage crops was clearly demonstrated. Also, the important role played by crop geometry was shown with regard to wheat and mustard classes. Late sown wheat, which has protruding structures, shows significant improvement within $m-\delta$ compared to the $m-\chi$ method for this class. We then show the reproducibility of major results using a different date CL-Pol data to over Junagad region of Gujarat. This work needs to be extended to crops at various phenological stages to understand the role and mechanism in which this data manifests the crop dynamics. To firmly establish the theoretical basis of many observations in this paper, CL-Pol decomposition over various landcovers is to be carried out.

ACKNOWLEDGMENT

This work is carried out with the data from RISAT data Utilization programme and authors are grateful to Dr. Manab Chakraborty, Project Director, RISAT-UP. Authors are thankful to Shri Tapan Misra, Director, Space Applications Centre, ISRO, Ahmedabad for his constant encouragement. The logistic support provided by Haryana State Remote Sensing Centre during field data collection is duly acknowledged.

REFERENCES

1. Raney, R. K., "Hybrid-polarimetry SAR architecture," *IEEE Trans. Geosci. Remote Sens.*, Vol. 45, No. 11, 3397–3404, Nov. 2007.
2. Raney, R. K., "Dual-polarized SAR and stokes parameters," *IEEE Geosci. Remote Sens. Lett.*, Vol. 3, No. 3, 317–319, Jul. 2006.
3. Charbonneau, F., "Compact polarimetry: General results," *Proceedings of the 2nd Compact Polarimetry Workshop*, Ottawa, Ont, January 6–7, 2009.
4. Charbonneau, F. J., B. Brisco, R. K. Raney, H. McNaim, C. Liu, P. W. Vachon, J. Shang, R. DeAbreau, C. Champagne, A. Merzouki, and T. Geldsetzer, "Compact polarimetry overview and applications assessment," *Can. J. Remote Sensing*, Vol. 36, S298–S315, 2010.
5. Dubois-Fernandez, P., J.-C. Souyris, S. Angelliaume, and F. Garestier, "The compact polarimetry alternative for spaceborne SAR at low frequency," *IEEE Trans. Geosci. Remote Sens.*, Vol. 46, 3208–3222, 2008.
6. Ainsworth, T. L., J. P Kelly, and J.-S. Lee, "Classification comparisons between dual-pol, compact polarimetry, and quad-pol imagery," *ISPRS Journal of Photogrammetry and Remote Sensing*, Vol. 64, No. 5, 464–471, 2009.
7. Lee, J. S., "Digital image enhancement and noise filtering by use of local statistics," *IEEE Transactions on Pattern Analysis and Machine Intelliegence*, Vol. 2, No. 2, 165–168, 1980.
8. Lee, J. S., "Refined filtering of image noise using local statistics," *Computer Vision, Graphics, and Image Processing*, Vol. 15, 380–389, 1981.
9. Lee, J. S., M. R. Grunes, and G. De Grandi, "Polarimetric SAR speckle filtering and its implication for classification," *IEEE Transactions of Geoscience and Remote Sensing*, Vol. 37, No. 5, 2363–2373, 1999.
10. Lee, J. S. and E. Pottier, *Polarimetric Radar Imaging: From Basics to Applications*, CRC Press, 2009.
11. Stratton, J. A., *Electromagnetic Theory*, McGraw-Hill, New York, 1941.
12. Raney, R. K., "Decomposition of hybrid-polarity SAR data," *PolIn-SAR 2007: Proceedings of the 3rd International Workshop on Science and Applications*, Frascati, Italy, January 22–26, 2007. H. Lacoste and L. Ouwehand (eds.), ESA Publications, *ESTEC*, SP-644, Noordwijk, The Netherlands, 2007.
13. Jayasri, P. V., H. S. V. Usha Sundari, E. V. S. Sita Kumari, and A. V. V. Prasad, "M-delta decomposition of hybrid dual-polarimetric RISAT-1 SAR data," *9th International Radar Symposium India*, 2013.
14. Lardeux, C., D. Niamen, J. B. Routier, A. Giraud, P. L. Frison, E. Pottier, and J. P. Rudant, "Assessment of compact polarimetry over different tropical environment and dataset," *Geoscience and Remote Sensing Symposium (IGARSS)*, 3279–3282, 2010.
15. Lardeux, C., P.-L. Frison, C. Tison, J.-C. Souyris, B. Stoll, B. Fruneau, and J.-P. Rudant, "Support vector machine for multifrequency SAR polarimetric data classification," *IEEE Trans. GRS*, Vol. 47, No. 12, 4143–4152, 2009.
16. Tapan, M., S. S. Rana, N. M. Desai, D. B. Dave, Rajeevjyoti, R. K. Arora, C. V. N. Rao, B. V. Bakori, R. Neelakantan, and J. G. Vachchani, "Synthetic Aperture Radar payload on-board RISAT-1: configuration, technology and performance," *Current Science*, Vol. 104, No. 4, 2013.

17. Haldar, D., A. Das, S. Mohan, O. Pal, R. S. Hooda, and M. Chakraborty, "Assessment of L-band SAR data at different polarization combinations for crop and other landuse classification," *Progress In Electromagnetics Research B*, Vol. 36, 303–321, 2012.
18. Haldar, D., M. Chakraborty, K. R. Manjunath, and J. S. Parihar, "Role of polarimetric SAR data for discrimination/biophysical parameters of crops based on canopy architecture," *Int. Arch. Photogramm. Remote Sens. Spatial Inf. Sci. XL-8, ISPRS Technical Commission VIII Symposium*, 737–744, Hyderabad, India, 2014.
19. Congalton, R. G., "A review of assessing the accuracy of classifications of remotely sensed data," *Remote Sens. Environ.*, Vol. 37, 35–46, 1991.
20. Kumar, V. and Y. S. Rao, "Comparative analysis of RISAT-1 and simulated RADARSAT-2 hybrid polarimetric SAR data for different land features," *Int. Arch. Photogramm. Remote Sens. Spatial Inf. Sci. XL-8, ISPRS Technical Commission VIII Symposium*, Hyderabad, India, 2014.